CIRP Journal of Manufacturing Science and Technology 40 (2023) 199–212

Contents lists available at ScienceDirect

CIRP Journal of Manufacturing Science and Technology

journal homepage: www.elsevier.com/locate/cirpj

Meeting high precision requirements of additively manufactured components through hybrid manufacturing

Alejandro Loyda [a,*], Mikel Arizmendi [a], Sergio Ruiz de Galarreta [a], Naiara Rodriguez-Florez [a,b], Amaia Jimenez [a]

[a] Universidad de Navarra, TECNUN Escuela de Ingeniería, Manuel Lardizábal 15, 20018 San Sebastián, Spain
[b] IKERBASQUE, Basque Foundation for Science, Plaza Euskadi 5, 48009 Bilbao, Spain

ARTICLE INFO

Available online 10 December 2022

Keywords:
Metal additive manufacturing
Additive hybrid manufacturing
Milling
Finite element (FE)
Residual stress simulation
Ti6Al4V

ABSTRACT

A hybrid approach combining the laser powder bed fusion (LPBF) process and post-processing operations through 5-axis milling was employed to manufacture a Ti6Al4V aerospace component. From the design step, the requirements and needs in all the stages of the Hybrid Additive Manufacturing process were taken into account. A numerical simulation of distortions promoted by residual stresses during the additive process was employed to consider material allowance. The status of the as-built and post-processed component was analysed through scanning and CMM inspection and roughness measurements. The 3D scanned model of the as-built LPBF-ed component was used to understand the distortion behaviour of the component and compared to the numerical simulation. Finally, 5-axis milling operations were conducted in some critical surfaces in order to improve surface quality and dimensional accuracy of the as-built component. The inspection of the as-built and post-processed component showed the improvement achieved through the proposed hybrid approach. The work aims to provide the baselines needed to enable the metal Hybrid Additive Manufacturing of components with complex geometries where mandatory precision is required by integrating high accuracy machining operations as post-processing technique.

Introduction

Metal additive manufacturing (AM) is changing the way components are designed and manufactured, since complex design with internal features, mass reduction and material efficiency can be achieved. As a consequence, additively manufactured components have gained interest in many fields such as the aerospace, biomedical and automotive industries. The generation of near-net-shape components makes AM more cost-efficient due to its waste minimisation. For instance, aircraft titanium components made by traditional methods present a buy-to-fly ratio of 12–25:1 [1]. Since any weight reduction results in lower fuel consumption and increases the load capacity of aircrafts, optimised components for AM methods have achieved a ratio of 3–12:1 [2]. Although AM has a remarkable and distinctive advantage over traditional subtractive machining methods, most of the additively manufactured components do not meet the required mechanical properties, geometrical and dimensional accuracy, and good surface finishing to be put into service. Dimensional and geometrical tolerances and surface roughness verification are critical stages in the manufacturing cycle since shape deviations and manufacturing imperfections could remain in individual parts and affect the performance of subsequent manufacturing stages. The literature has shown that post-processing machining operations can enhance surface quality and dimensional and geometrical accuracy of additively manufactured components. This combination of additive and subtractive technologies is commonly known as Hybrid Additive Manufacturing [3].

Most of the defects induced by AM are inherent to the process itself. As the material is deposited layer-by-layer, a stair-step effect is generated on the surface. In this regard, layer thickness plays a major role in controlling surface roughness values [4,5]. Moreover, partially melted powder and unmelted powder bond to the surrounding surfaces due to the influence of the high temperatures that arise during printing, resulting in the generation of surface imperfections [6]. Besides, when the support structures are removed, the remaining traces greatly deteriorate the surface morphology and quality. As Jiménez et al. [7] pointed out, most of the AM components need some post-processing, since a stand-alone AM technology presents several limitations for producing functional parts. Thus, by integrating post-processing operations in the

* Corresponding author.
E-mail address: aloydaquiro@tecnun.es (A. Loyda).

https://doi.org/10.1016/j.cirpj.2022.11.011

manufacturing of those components, their mechanical properties, dimensional accuracy and surface integrity can be improved.

Among the different metal AM technologies, laser powder bed fusion (LPBF) technology is probably the most common. LPBF is capable of fusing a wide range of materials, tuning properties during the processing of the components depending on the requirements and improving the building rate by introducing multiple laser sources [8]. However, because of the successive heating and cooling cycles generated in the deposited layers, the LPBF process involves high thermal gradients, which leads to non-uniform surface heating and rapid solidification and cooling rates. Additionally, these thermal cycles introduce residual stresses, which induce undesired distortions on the built parts [9]. As a result, geometrical inaccuracy, cracking, warping, layer delamination, reduced fatigue performance and anisotropic mechanical behaviour are prompted [10].

In order to control and optimise AM process performance and results, researchers have simulated numerically different phenomena that occurs during the process. Thermo-mechanical finite element simulation aiming at predicting residual stresses and distortions has been used to investigate the complex additive behaviour. Distortions of LPBF-ed components tends to be a macroscopic phenomenon [11], therefore, the geometry of the LPBF-ed components is an influencing aspect which cannot be neglected or simplified. Although at macroscopic level the thermal behaviour is affected by a great number of conditions. The thermal gradient mechanism (TGM) based on the thermal expansion and contraction behaviour during heating once the laser irradiates and cooling once it moves away, respectively, and a cool-down phase have given a knowledge about the distortions due to residual stresses [12–14]. At heating stage, the laser beam heats up the fed stock powder on the upper layer by forming a melt pool. The material expands thermally, but this expansion is limited by the colder surrounding material of the underlying layers, inducing elastic compressive stresses in the heat affected zone below the melt pool. Consequently, the material's yield strength lowers as result of increasing temperature, promoting a non-uniform plastic deformation on the heated material. At cooling stage, the melted material begins to solidify and shrinks owing to thermal contraction; however, the shrinkage is partially inhibited due to the different rates of cooling throughout the layers. Thus, the farthest portion of the heat affected zone cools and contracts first, compressing the warmer inner portion, and when the inner portion tries to contract, it is constrained by the already cooler portion. Consequently, a portion keeps tensile residual stresses while the portion below keeps compressive residual stresses. Due to the fact that the number of layers keeps increasing, the irradiation of each new layer laid on the top makes it likely that the recently subjacent solidified layers will re-melt and re-solidify (or reach high temperatures again). Thus, the warmer regions contract to a greater extent than the colder regions. Due to the inhibition, most of the resulting tensile residual stresses turn into compressive stresses as the distance from molten zone increases. As the height raises progressively by the layers to build the component, compressive stresses tend to occur at the bottom of the part [12]. Finally, at a cool-down phase after printing, the component is removed from the build platform, and a stress relaxation process (springback phenomenon) takes place [12,15,16]. Shipley et al. [17] summarised how numerous conventional and alternative processing parameters can be optimised to address inherent defects of the metal AM process, such as porosity, microstructure and residual stress. In addition, authors questioned the validity of using the energy density equation as a means of process characterisation by showing the variance in porosity for components processed at the same energy density. Xiao et al. [10] validated a 3D finite element model with experimental results under different scanning speed and laser power values to analyse their influence on residual stresses during LPBF of Ti6Al4V. They noted that the scanning speed has greater influence than the laser power on the residual stresses.

The present research is focused on Ti6Al4V, an $\alpha + \beta$ titanium alloy with low density, high strength, excellent corrosion resistance and high fracture toughness. It is also biocompatible and extremely suitable for many airframe components and surgical implants [9,18]. In addition, AM capabilities can make most of its well-known high specific strength (strength-to-weight ratio) by saving weight where load structures are required. However, working with Ti6Al4V is challenging due to its tendency to strain hardening and chemical reactivity to oxygen [19–21]. Moreover, the phase transformation of Ti6Al4V is strongly affected by the temperature history and cooling rates. In this regard, it is known that α' martensite phase results from most of the powder bed fusion methods such as LPBF, causing an anisotropy which in turns affects the ductility of the material [22–25]. Additionally, since the powder bed can be considered as a porous medium material consisting of bulk material and infiltering gas, and the rapid temperature change thermophysical properties such as the density, thermal conductivity and enthalpy of the metal powder materials are considerably different from those of bulk. Although it is difficult to estimate the exact values of the temperature-dependent properties of the metal powder, its consideration plays an important role in the part deformation prediction [26].

Material removal post-processes such as milling are capable to improve the superficial and geometrical imperfections by even subtracting a thin layer of material, however, material mechanical properties, geometry and mounting strategy can aggravate the performance. Ti6Al4V is known to have a low machinability as a consequence of its low thermal conductivity, low elastic modulus and maintenance of its strength and hardness at elevated temperatures. These properties can result in rapid tool wear, non-uniform material removal and degradation of surface integrity [27,28], which might cause surface damage and reduce fatigue life [29]. Additionally, the LPBF process add anisotropic mechanical properties to the Ti6Al4V alloy [21]. Ni et al. [5] compared the sensitivity of cutting speeds to surface roughness of LPBF-ed Ti6Al4V alloys and concluded that sensitivity is much greater than to annealed Ti6Al4V alloys. Besides, different roughness values were detected on the surfaces of the LPBF-ed Ti6Al4V samples. Maleki et al. [30] discussed surface post-processing methods to address the issues associated with the irregular surface morphology of as-built AM metallic parts. The access to the surface, and the size and shape were aspects to consider in choosing the applied post-processing. They highlighted the contradictory effects that can be induced by certain treatments such as tensile residual stresses and over-alteration on geometrical aspect, if not finely controllable. The comparison of surface post-treatments showed that material removal methods reach the better improvement in roughness reduction and are able to remove pores located on the surface. Internal channels or holes are characteristics in most of the components that join to a structure, therefore, their construction and precision play an important role. Pakkanen et al. [31] showed the main problems in internal channels manufactured by LPBF such as the high surface roughness and the distortion of the shape, the defects varied from material and printing orientation. Although, orientations are suggested to reduce such defects, the precision is far to be reached and bring the need of Hybrid Additive Manufacturing.

Recently, hybrid workflows have been presented to enhance the capabilities of adding a subtractive stage. Zhang et al. [32] worked on a case of study of a blade that was simplified as a cantilever thin plate through Hybrid Additive Manufacturing. The two-step machining achieved a better surface roughness below 0.815 µm and showed that residual stress after machining was compressive stress. However, they concluded that the proposed method cannot eliminate surface errors and may be unable to handle complex parts. Since it could be only transferred to thin-walled LPBF-ed parts. Yaghi et al. [33] presented a method to design a component against distortion for AM, at the first stage, a non-compensated component was

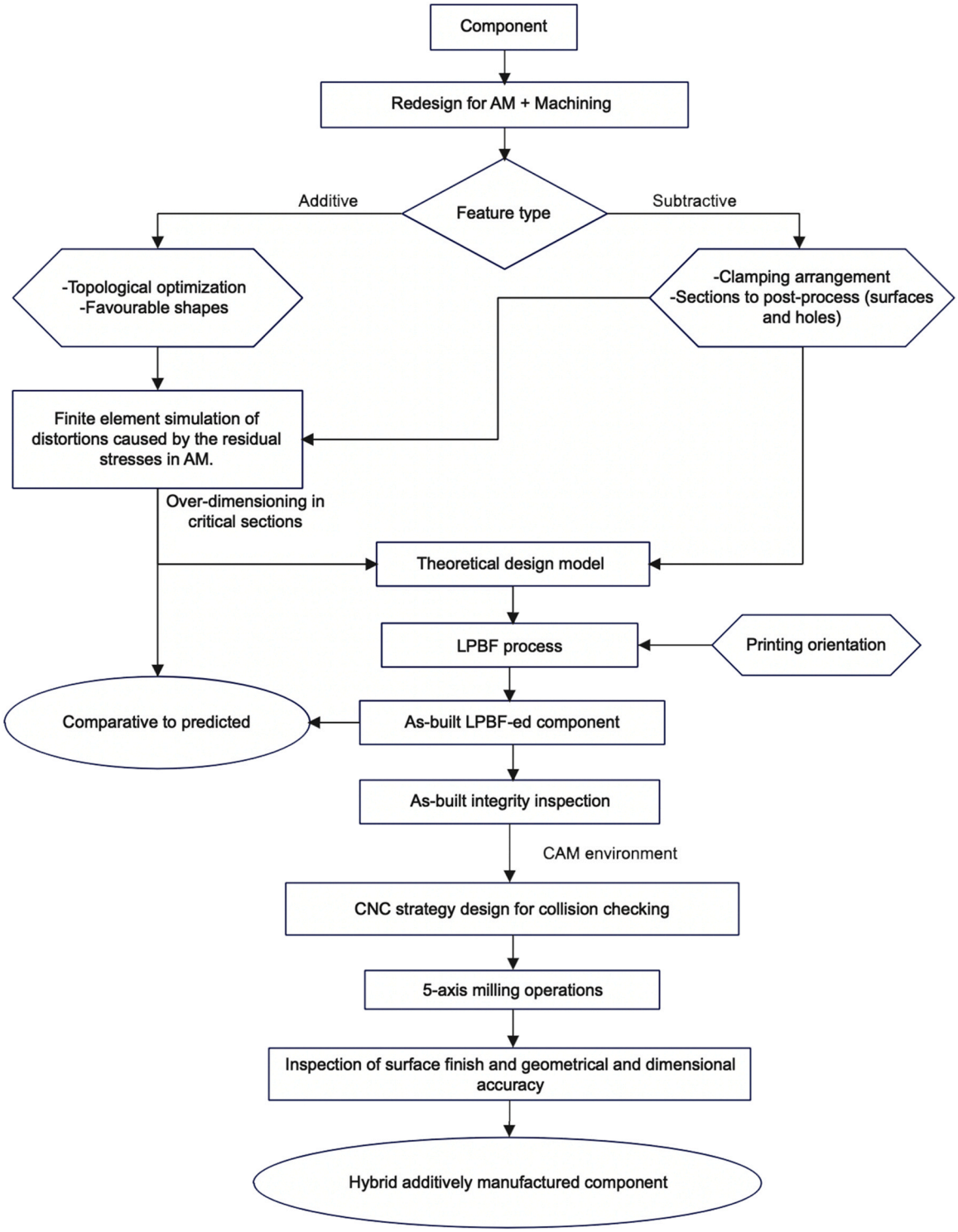

Fig. 1. Proposed hybrid approach to manufacture any complex shape.

manufactured by AM and post-machined removing around 0.5 mm from certain surfaces. The distortions were measured and numerically simulated. At the second stage, a distortion-compensation procedure was applied, which consisted in taking the distorted simulated mesh to compensate the model to print in the opposite direction for the actual distortion that occurs when the AM process takes place. The distortions in the new component have a reduction to less than 50% of the original non-compensated values. However, this method represents to increase the cost, manufacturing time and use of material.

Despite the great advances in metal AM, the transition from traditional processes to AM production is still restricted. Complex cases of study aimed at improving the dimensional accuracy and surface finish of AM-ed parts through Hybrid Additive Manufacturing are rarely reported. Given this context, a hybrid approach that integrates subsequently metal AM and machining through 5-axis milling is presented in this paper to manufacture a Ti6Al4V load-bearing bracket. The proposed solution takes in account the needs of the machining process from component design stage. A comprehensive study was driven by intermediate inspection

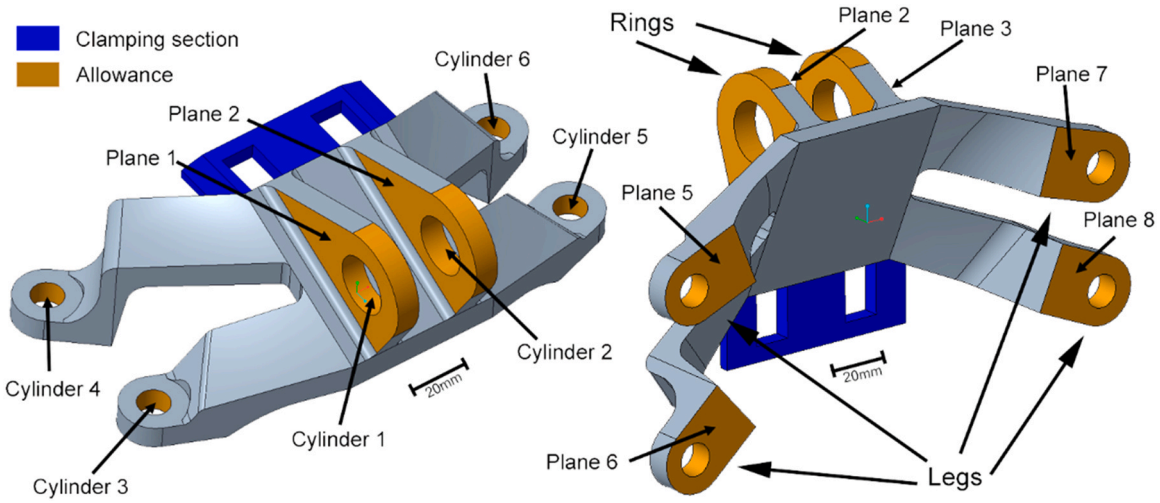

Fig. 2. Theoretical model used to print the component by LPBF marked with the clamping section and the set-up allowance. And sections in which dimensional and geometrical tolerances were measured.

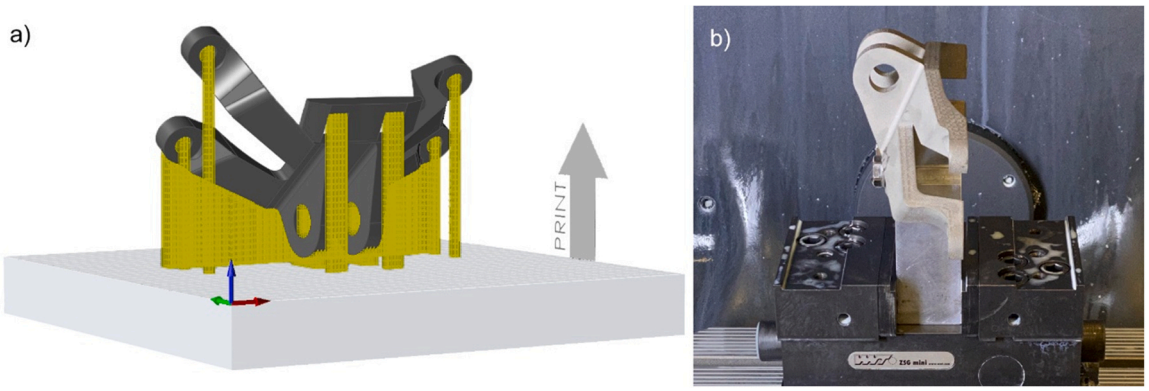

Fig. 3. Studied component: a) schematic diagram of the orientation and the support material employed in the LPBF process and b) as-built Ti6Al4V component mounted into the CNC machining centre.

stages to analyse effects of the LPBF process on the generated geometry as well as the achieved part quality after post-processing. The Hybrid Additive Manufacturing workflow suggested in this study can be extended to other additively manufactured metal components where high precision is required.

Methodology

Hybrid Additive Manufacturing can be approached together with Design for Manufacturing (DFM) strategies, in which manufacturing constraints and sustainability needs are as important as the product itself. AM is not constrained by manufacturing limitations such as the shape, but the accuracy. By joining subtractive operations in a sequential process, the quality of a component is improved and the productivity and efficiency of the process are enhanced. The workflow that summarised the approach proposed in this work is outlined in Fig. 1. It is important to note here that in this hybrid approach both AM and 5-axis milling requirements were considered from the component design stage, as it will be shown in the next sections, some additional features where added to the original design in order to ensure tool accessibility and a rigid clamping during the post-processing stage.

In this work, an aeronautical bracket, which is an example of load-bearing structures for mounting application in aircraft engine, was chosen to manufacture through the proposed hybrid approach. The starting model was based on an open-source GE loading bracket made of Ti6Al4V [34]. As AM enables the generation of complex geometries, a topological optimisation (TO) analysis was integrated in the proposed approach to generate an appropriate design. The resulting geometry obtained in this TO study was employed later as guide to generate the final design of the bracket. The commercial software Altair HyperWorks was used to carry out the TO. Two regions were established to represent the designable and non-designable regions. Besides, a minimum element size was adopted to avoid unconnected sections and a constraint of maximum yield strength.

An original design was created by redesigning the optimised light-weight model using the CAD tools of the commercial software CREO Parametric to shape some geometrically favourable features for AM [35]. As mentioned, working with DFM demands to consider transcendental features from the conceptual design, although this means to slightly maximise the use of material, the post-processing time can be reduced. Hence, to clamp and mount the as-built component into the CNC machine, a section was added too in the redesign to ease the operation in a single set-up. The original design of the component and the added clamping features are presented in Fig. 2.

Then, a finite element simulation to predict the distortion due to residual stresses was conducted. Based on this analysis, an allowance or over dimensioning was adopted in the original design to meet the final dimensional specifications of the component in areas of connection and subjection, identified as critical part surfaces. Hence, a

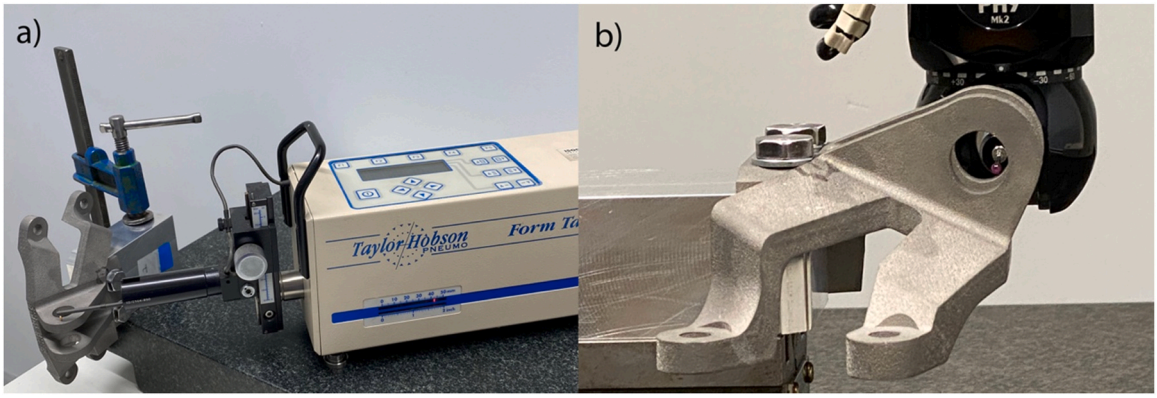

Fig. 4. Inspection of the as-built Ti6Al4V component using a) a Taylor-Hobson profilometer to acquire the roughness profiles and b) a DEA Mistral CMM to quantity the dimensional accuracy.

Table 1
Cutting tool specifications.

Tool type	Cutter diameter (mm)	Corner radius (mm)
End mill	10	–
End mill	8	–
Bull mill	16	3

final theoretical design (named as over-dimensioned part) of the bracket with complex shape was set up as the case of study. Fig. 2 presents the theoretical design along with specifications about the terms that will be employed in this paper to refer to different component features.

Through the finite element simulation, it was possible to evaluate different printing orientations and support structure location before the additive manufacturing of the original component. Fig. 3a shows the orientation and the support material employed during the LPBF process. The LPBF-ed component was separated from the substrate and the first inspection analysis was carried out. The as-built component was scanned and compared with the results from the numerical model to draw comparisons between the simulation and the experiments. Additionally, surface roughness of the as-built component along with dimensional and geometrical characteristics of different sections were also measured. The average surface roughness (Ra) was calculated by means of roughness profiles measured on numerous surfaces.

Lastly, in Fig. 3b the machining set-up is shown. As it is observed, a metallic component was added to the set-up in order to improve tool accessibility and to avoid possible collisions during machining. The CAM module of the commercial software CREO Parametric was used to define the machining strategies. Once the machining stage was completed, the surface integrity and dimensional and geometrical accuracy were analysed again on the post-processed component.

In the following sections, further details about the steps followed in this hybrid approach will be presented.

Simulation of the LPBF process

The AM deposition of the Ti6Al4V powder particles of the studied component was numerically simulated by importing a set-up model of the topologically optimised design into the commercial software Altair Inspire Print3D. A thermo-mechanical finite element analysis of the LPBF was conducted with a laser power of 500 W, a scanning speed of 1200 mm/s, layer thickness of 60 µm and a cooling period of 600 s at room temperature. The temperature-dependent thermophysical and mechanical properties of the Ti6Al4V powder and fused material were considered in the software for the simulation [36,37]. The model consisted of a three-stage approach; printing, cooling and springback, to retrieve the residual stresses distribution and the distortion of the component. It was assumed that the component with fixed support structures was attached to the building platform until the last layer was deposited for the printing and cooling simulations. For the springback stage, the substrate and the support structures were removed from the as-built component. The numerically simulated residual von Mises stresses were calculated at the end of each stage. The colour bar limits were fitted to the maximum and minimum stress values among different stages (printing, cooling and springback) to ease the comparison of the distribution change. The analysis of the distortion generated in the component was conducted in the last stage, once it was separated from the substrate.

LPBF process

Ti6Al4V ELI alloy (with extra low interstitials, ASTM Grade 23) powder was used for the AM of the aerospace component. This higher purity version of Ti6Al4V with the chemical composition (wt %): Ti (Balance), Al (5.50–6.50), V (3.50–4.50), Fe (≤ 0.25), O (≤ 0.13), C (≤ 0.08), N (≤ 0.05) and Y (≤ 0.005) provides improved ductility and better fracture toughness due to lower inclusions of iron and interstitial elements, carbon, nitrogen and oxygen [38]. During manufacturing, layer thickness was set to 60 µm. The component was printed in a Renishaw RenAM 500 M LPBF machine equipped with a

Table 2
Cutting parameters employed during 5-axis milling operation.

Operation	Section	Cutter	Feed rate (mm/min)	Cutting Speed (m/min)	Step over (mm)	Step depth (mm)
Finishing	Side surfaces of rings	Bull mill 16	250	60.31	–	6
Roughing	Holes of rings	End mill 10	300	50.26	2	–
Finishing	Holes of rings	End mill 10	250	50.26	2	–
Finishing	Upper surfaces of rings	End mill 10	250	50.26	–	15
Finishing	Bottom surfaces of bases	End mill 10	200	47.12	6	–
Finishing	Holes for bolts	End mill 8	250	37.69	1	–

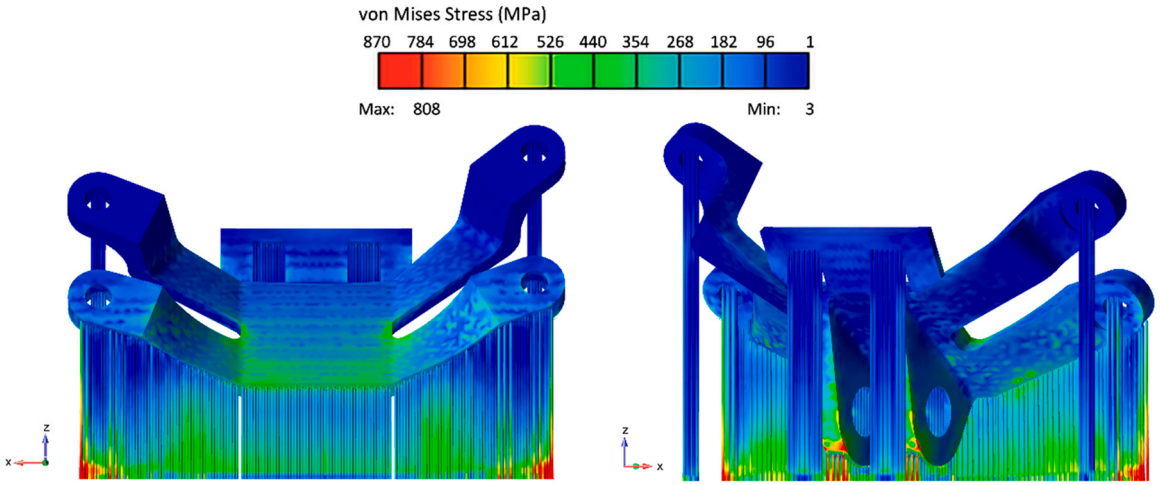

Fig. 5. Residual von Mises stresses of the studied component at the end of the printing stage.

built chamber of 250 mm × 250 mm x 350 mm and ytterbium fibre laser that can irradiate a maximum power of 500 W. In order to prevent oxidation, the build chamber was filled with argon gas during the AM process. Electric-Discharge Machining (EDM) was used to remove the as-built LPBF-ed component from the substrate.

Component inspection

In order to study the geometrical accuracy of the LPBF process, a 3D model of the as-built component was generated using the HandyScan H3D300 manual scanner with a measure area of 225 × 250 mm, an error tolerance of 0.100 mm and recording of 205 000 measures/s. Vxscan, VxModel and VxInspect software was used to compare to theoretical model with the measured data. Additionally, the surface roughness was measured by means of a Taylor-Hobson profilometer model (Form Talysurf Plus with stylus radius of 2 µm) and a sampling length of 8 mm. Roughness profiles were acquired on different regions and the Ra of the roughness were computed. By using a DEA Mistral coordinate measuring machine (CMM), model 07.07.05, with useful races of X = 710 mm, Y = 660 mm and Z = 460 mm, dimensional deviations, hole diameters and thicknesses were measured and compared between the as-built and post-processed components. Also, the flatness, parallelism and perpendicularity deviation was measured in terms of distance to the indicated reference. Fig. 4 shows the equipment used to measure the surface roughness and dimensional and geometrical accuracy.

Five-axis milling

With a focus on the post-processing of the as-built bracket, the finishing of the functional surfaces together with the cutting tools (Table 1) were defined with the CAM tools of Creo Parametric through 5-axis milling operations. In addition, the cutting parameters shown in Table 2 were established to perform the machining operations of the sections marked in Fig. 2. Since Ti6Al4V is a difficult-to-machine metal, low cutting speeds were chosen to minimise tool edge temperature, and plentiful amounts of cutting fluid were used to reduce heat and improve chip evacuation [27,29,39]. A 5-axis DMG DMU50 CNC vertical machining centre was employed for the machining.

Results and discussion

Residual stresses and distortion of the as-built component

Simulation of residual stresses and distortions through FE model

Residual von Mises stresses predicted immediately after the last layer was deposited at the end of the printing stage are shown in Fig. 5. During LPBF the part was exposed to thermal stresses due to

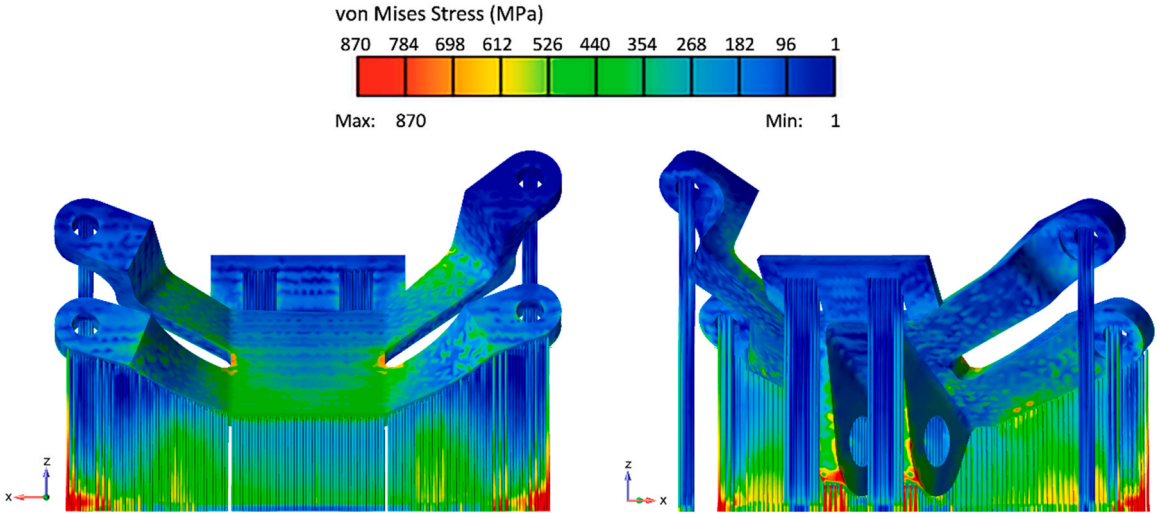

Fig. 6. Residual von Mises stresses of the studied component after the cooling stage.

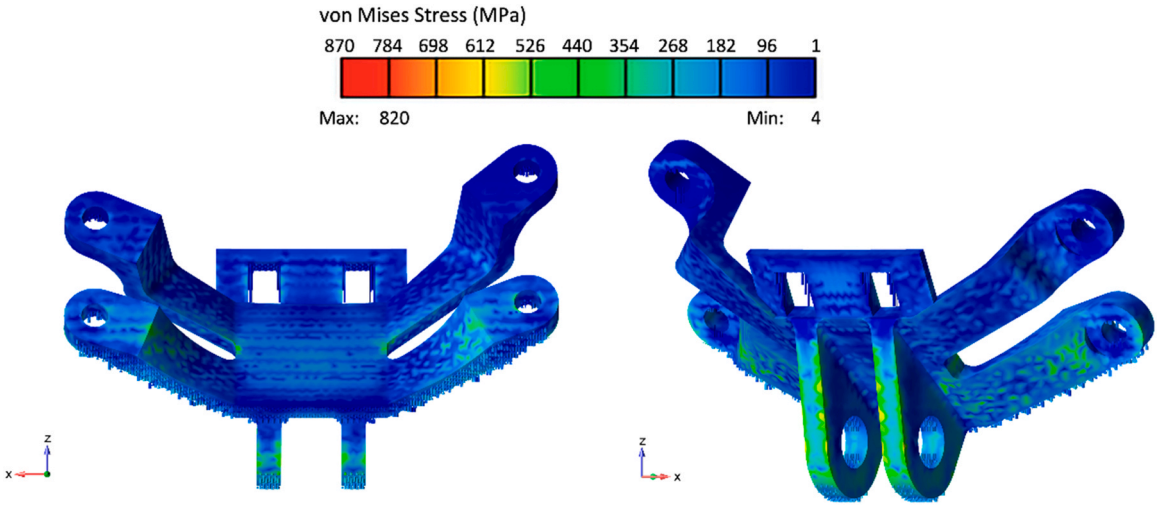

Fig. 7. Residual von Mises stresses of the studied component after the springback stage.

the large thermal gradients caused by rapid heating and solidification of melted powders. As more layers were stocked and constrained in the Z direction, the increase of the reheated material resulted in the accumulation of the residual stress. It can be seen in the figure that the constraint regions in the component experienced the maximum stress values (over 808 MPa on the edges of the rings). The stress is relatively low in the last layers at the top. This result agrees with what has been reported in the literature. As shown by Hussein et al. the powder at the bottom contributes to a higher cooling rate and solidification at the side of the layer compared to the upper, resulting in higher residual stresses at the bottom [40]. In this case, the highest stress values were predicted at the bottom where colder layers are located.

The residual von Mises stresses distribution after the cooling period is presented in Fig. 6. At this stage, the values above 268 MPa covered a larger region on the component (coloured in green colour), mostly at the centre and the legs. The stress distribution is not symmetric, particularly in the centre, due to the scanning pattern and residual heat. It has been assumed in previous studies [41], that the residual stress in the scanning pattern direction is generally larger than the other two directions. The whole component tended to shrink due to the thermal contraction, but the solid metallurgical bonding between layers avoided an actual shrinkage. However, this induced an increase of stresses with respect to the as-deposited status (Fig. 5). It is worth noting that the higher residual von Mises stress at certain edge regions, which were still constrained by the supports, reached values in the range of 700–870 MPa. Given these values, plastic deformation of the component could occur in these regions (note that the anisotropic yield stress of LPBF-ed Ti6Al4V is in the range of 850–1100 MPa [9]). In the four legs of the component, a remarkable change on stress values from previous stage was presented in the connection of the bases with the centre: 339 MPa where reached as opposed to the 113 MPa obtained before. It is seen that the top of the component was subjected to a lighter residual stress accumulation (about 87 MPa).

Fig. 7 illustrates the residual von Misses stresses once the component was separated from the built platform. The remaining stresses from previous stage caused a warping phenomenon as a part of the stress is relieved after it is cut off from the substrate. The stress distribution in the component drastically changed as the resulting stresses decreased due to the relaxation. The fitted colour bars limits allow to analyse how the stresses spread in the component from the previous stages. The stress release in the overhanging features (such as the whole legs) reached lower values around 96 MPa as opposed to the 339 MPa obtained before. However, the edges of the rings maintained values similar to those observed in previous simulations, due to the effect of the high temperature gradient and the constraint of the adjacent solidified support material.

The numerically predicted distortion along the X and Z directions at the final stage (springback) is shown in Fig. 8. It can be seen in the figure that the legs are more susceptible to distortion than any other

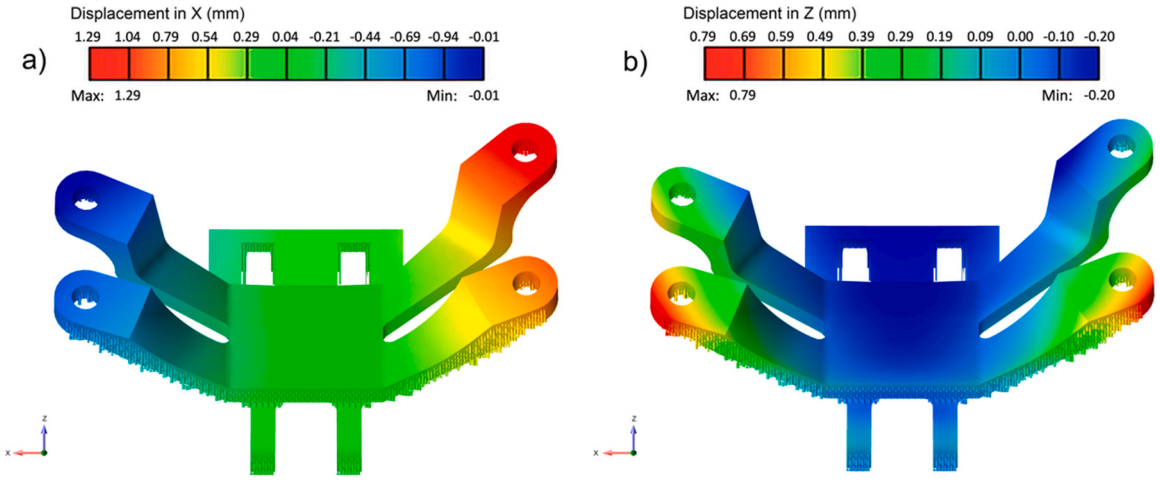

Fig. 8. Predicted distortion in a) X direction and b) Z direction of the studied component after springback.

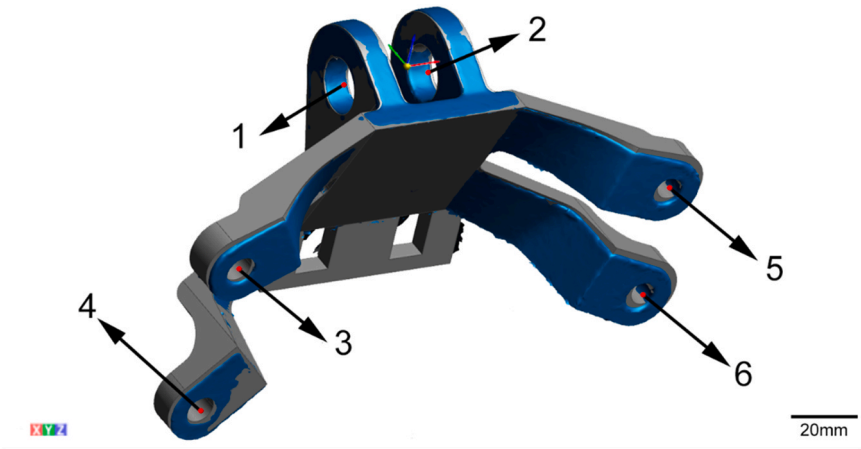

	Hole # deviation (mm)					
Direction	1	2	3	4	5	6
X	0.085	-0.331	1.093	0.931	-1.546	-1.779
Y	0.048	-0.023	-0.903	-0.108	-1.247	-0.696
Z	0.035	0.035	-0.804	-0.519	-1.226	-0.946

Fig. 9. Deviations of different sections of the as-built Ti6Al4V component in X, Y, and Z direction obtained by comparing the 3D scanned model (blue) with the theoretical model (grey).

region in the component. Distortion in Z represents the layer stacking direction while X direction represents the direction of recoating along to the substrate. Thus, it can be concluded that the warping direction followed an inward and upward trend.

Although the rings section accumulated higher amount of residual stresses, this section was slightly distorted because of its higher stiffness. It has been stated that support structures can mitigate the effect of thermal stresses and shrinkage on the component [42]. However, in the case of the lower legs, despite being completely constrained by the support structure, the distortions were greater than in the upper legs. A lower heat dissipation due to the overuse of support structure along the entire overhang area of the lower legs may be responsible for this behaviour.

Measured distortions

Fig. 9 presents a comparison of the shape of the as-built component (coloured in blue) to the theoretical model (shown in grey) to quantify the deviation in three directions. In order to analyse the

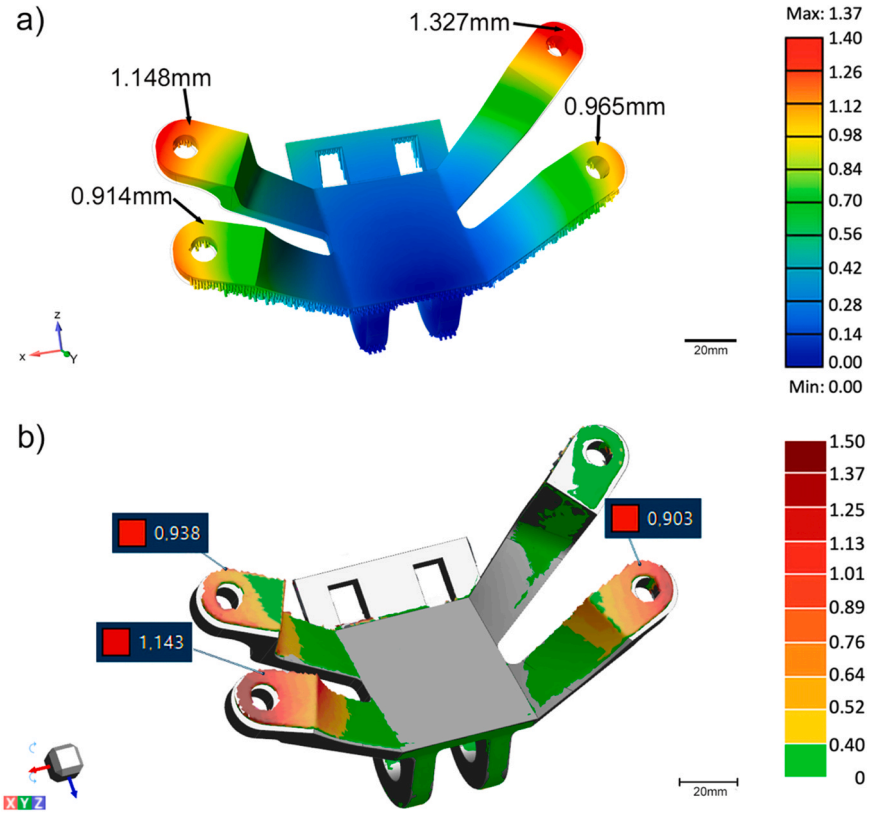

Fig. 10. Comparison of a) finite element predicted and b) experimentally measured deviations in mm.

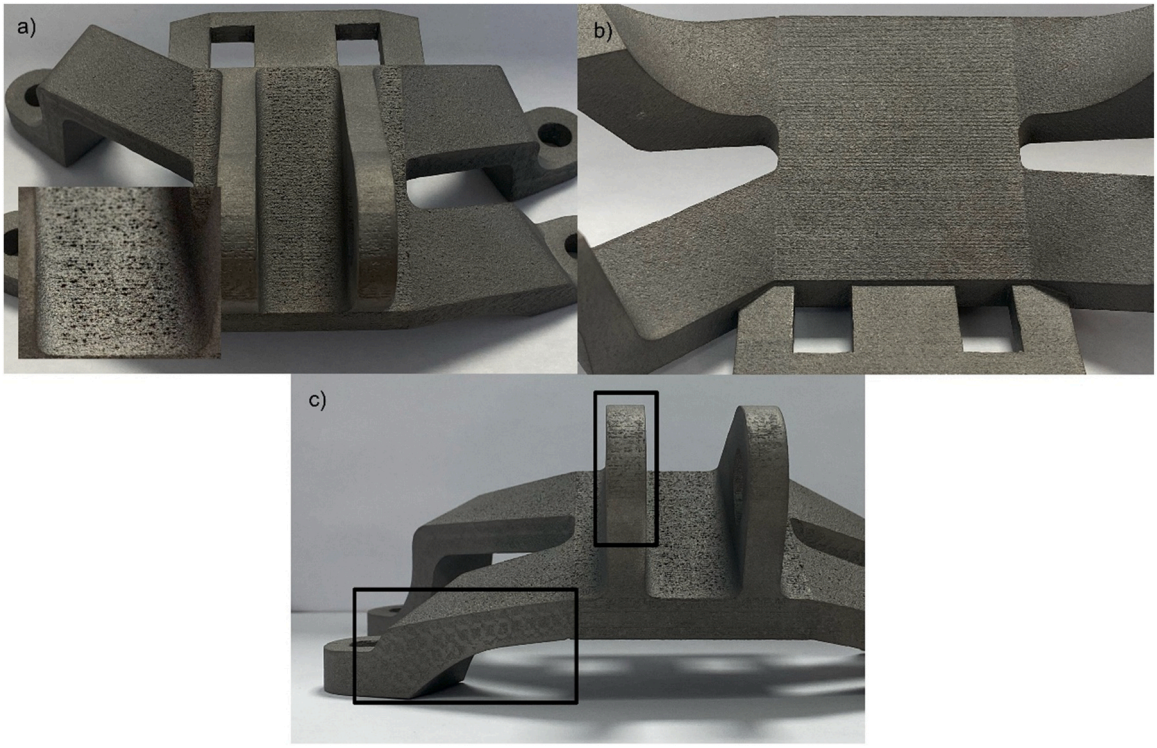

Fig. 11. Defects on the surface of the as-built Ti6Al4V component due to: a) bonding of unmelted powders, b) stair-step effect and c) trace of supports.

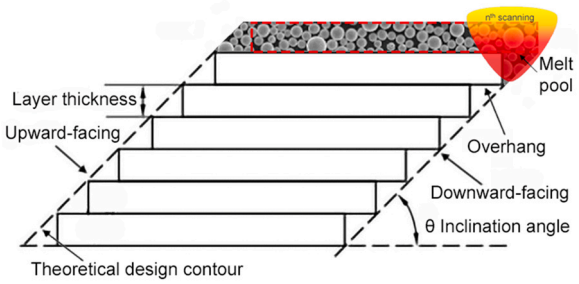

Fig. 12. Exemplification of facing position´s effects.

influence of the phenomena mentioned above, the 3D scanned model was oriented according to its in-service position. Data included in the table corresponds to measurements in the points in red, which were defined as the intersection between a plane and the cylindrical holes. The largest deviations occurred in the free ends of the legs**.** From this comparison, it can be extracted that a remarkable distortion occurred in X direction. For instance, in holes 5 and 6 the deviation was up to 1.546 mm and 1.779 mm, respectively. Two regions can be distinguished that show different deformation behaviours: (1) a barely affected region on the rings and (2) a greatly distorted region on the legs that was also predicted in the simulations and that is due to the residual thermal stresses and springback phenomenon generated during the manufacturing process.

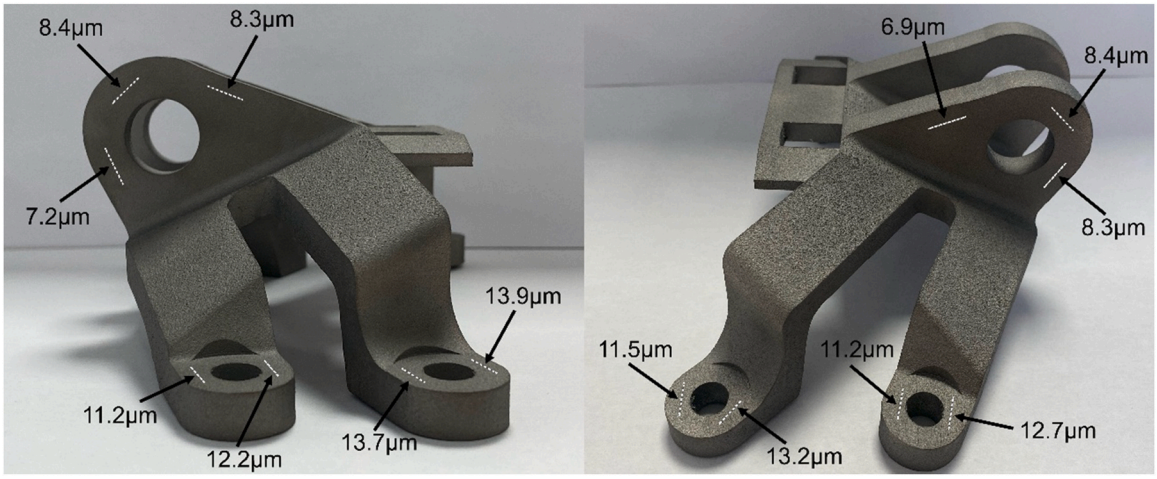

Fig. 13. Detail of the measured profiles and the average surface roughness (Ra) obtained on different surfaces of the as-built Ti6Al4V component.

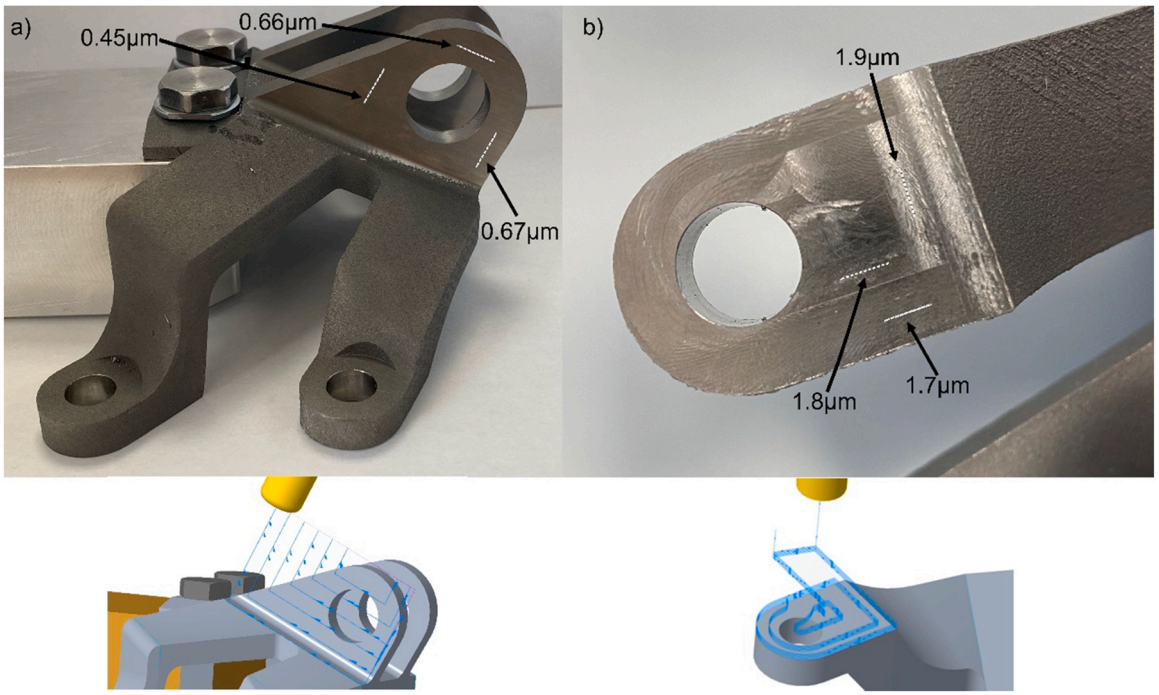

Fig. 14. Some of the measured profiles used to evaluate the average surface roughness after milling on surfaces of the additively manufactured Ti6Al4V component, below the tool path defined for each operation.

The absolute displacement of both the numerically predicted model and the experimentally measured component is shown in Fig. 10. By comparing these results, it was observed that the legs behaved similarly. The magnitude of the displacement in the free ends of the legs in both cases lays between 0.64 mm and 1.374 mm. Deviations predicted in three of these legs presented a good agreement with the experimental results. In general, it is observed that the simulation slightly underestimates the distortions of the LPBF process of the component, but it is able to qualitatively predict the behaviour.

Surface integrity

The as-built Ti6Al4V component is shown in Fig. 11. Non-uniform surface texture was easily noticed, which is caused by the bonding of unmelted powder, among other phenomena (Fig. 11a) [43]. In addition, the stair-step effect is also noticeable because of the layered nature of AM, as shown on the surface in Fig. 11b. Lines clearly demonstrate the printing tracks followed by the laser during LPBF. Layer thickness and printing orientation are the main reasons for this. Therefore, these defects are nearly impossible to mitigate, since an increase or decrease of the stair-step effect and its phenomena depend on the inclination angle. Support structures are important features in AM as they anchor the component to the build platform, conduct heat and prevent the sinking of molten metal. However, once the support structures were removed, they left traces along the surfaces. Fig. 11c shows a detail of these defects which greatly deteriorate the surface quality of the Ti6Al4V component.

Results exposed that the printing orientation had a great influence on the surface roughness. This difference in roughness depending on the inclination of the surface can be explained by Fig. 12. Once the laser beam heats the overhang area in Fig. 12, a large melt pool is formed and extended into the surrounding loose powder by the action of gravity and capillary forces. A region of the molten pool is in contact with the solid part and the rest is unsupported and surrounded with loose powder. Two or three layers might be exposed into the melt pool. Thus, during the solidification, the semi-melted powder particles are regularly absorbed and attached to the surfaces. If the build angle increases, the overhang is shortened and the molten pool is provided with a better support from the underneath solid layer. The influence of the scanning direction, whether parallel or perpendicular to the overhang, has been reported as not significant [44,45]. Thus, the roughness values largely differ between the surfaces that were generated at different angles of inclination, those differences rose standard deviation to 10.88%. When comparing two inclined surfaces at certain orientation the standard deviation was 2.27%.

Fig. 12 shows an exemplification of two kinds of inclined surface that can be identified, downward or upward-facing to substrate, in the arrangement to print. Ra values on the surface shown in Fig. 11a, which is an inclined downward-facing surface, are in the range of 28.6–32.8 µm. By contrast, in the surface shown in Fig. 11b, which is an inclined upward-facing surface parallel to the previous (Fig. 11a), the stair-step effect is noticeable and the Ra values are lower, between 18.5 µm and 22.5 µm. At this orientation, the underlying powder bed is supported and the surface roughness only depends on the stepping and the overhanging surface created by the build angle. As can be seen, a downward-facing surface tends to have a higher surface roughness and is more susceptible to deterioration.

Fig. 13 shows the roughness values measured on the four inclined downward-facing surfaces where the bolts are meant to join. Ra values are lower, ranging between 11.2 µm and 13.2 µm, since the built angle was less pronounced here. The lowest Ra values, in the range of 7.2–9.1 µm, were found on the lateral surfaces of the upper rings. These surfaces were printed perpendicularly to the build platform. At this orientation, the stair-step effect is less prominent and the overlap between successive layers plays a major role in the surface roughness. Although it may seem that a change in orientation could improve this roughness results. It is worth noting that orientation greatly affects residual stresses fields generated and the need for supports. Therefore, the optimisation of the component orientation should not be focused on optimising roughness, but in reducing residual stresses and support material needed.

Despite the deviations developed by the legs, all intended post-processing milling operations were carried out to achieve a better

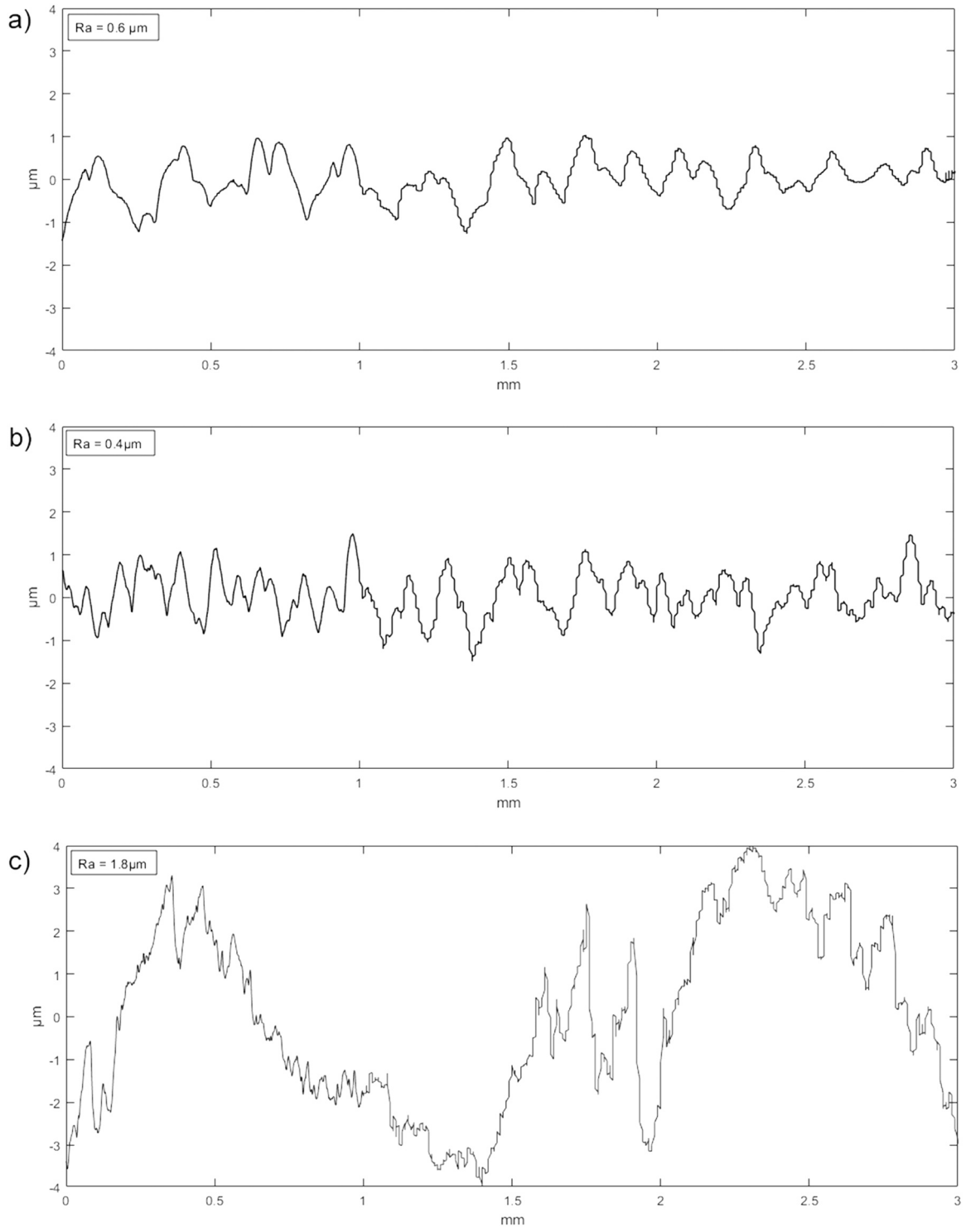

Fig. 15. Roughness profiles measured on different surfaces after profile milling in a) parallel to the tool path and b) perpendicular to the tool path and c) after a roughing operation over tool path.

surface finish and dimensional accuracy on the studied sections. It is worth noting that even though the deformations of the as-printed component were significant, the allowance set in the original model enabled the machining to be conducted properly. Fig. 14 shows two post-processed surfaces and a detail of the location of the measured profiles. Additionally, the corresponding tool paths are illustrated. As a reference, for cast or wrought components the standard guidelines for surface qualities for aerospace applications typically call for a surface roughness of Ra = 3.2 µm or even lower [46]. Clearly, the surface integrity of the post-processed component presented a better quality. The Ra values of the lateral surfaces of the rings (Fig. 14a) were below 1 µm, which proves that surface quality can be improved through Hybrid Additive Manufacturing. Roughness values measured on the base surfaces (Fig. 14b) were slightly higher, but still below 2 µm. Despite the fact that these sections were less stiff than the rings during the machining stage, which was meant to promote an instability of the machining operation, the strategy adopted overcame the problem. The Ra values of the bases were

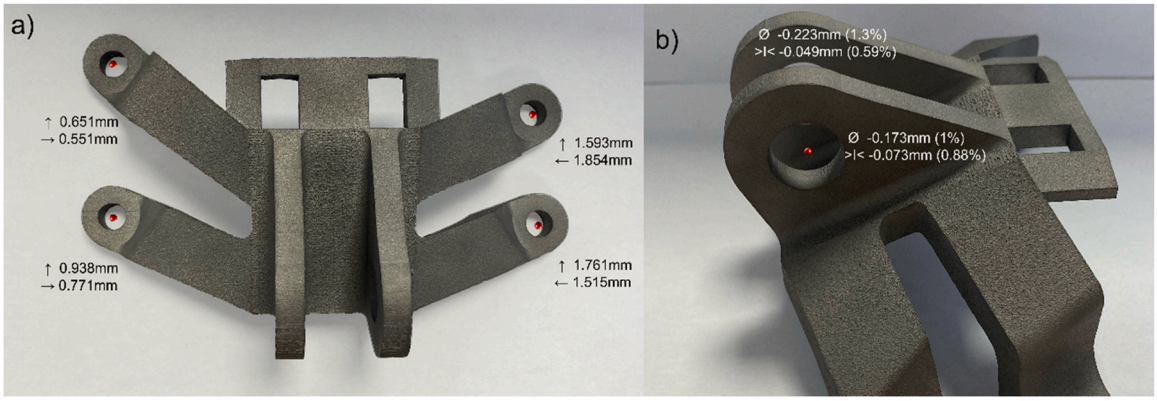

Fig. 16. Inspection of as-built component by means of MMC: a) deviation direction with values (mm) from original position, and b) difference of diameter and thickness to the theoretical model.

about 1.5–2 µm. Since the aim of metal AM is to print complex lightweight shapes, a major challenge to carry out machining operations on these parts is the poor support of the overhang sections when the component is clamped.

The complex design of the part played an important role on the milling performance since overhang and thin sections were machined. To briefly analyse the stability of the machining process, roughness profiles in two different post-processed surfaces were measured. Fig. 15a and b show the roughness profiles on the lateral surface of a ring (Fig. 14a) that was milled with the bull mill through a profile milling operation. These profiles were measured parallel (Fig. 15a) and perpendicular (Fig. 15b) to the tool path. Although it is difficult to extract a pattern from the obtained profiles, no undulations are perceived. Peaks that could correspond to the pass of cutting edges of the tool are observed. It can be concluded that the machining process performance was stable. Fig. 15c shows the roughness profile of a surface in the base of the component (Fig. 14b), that was milled with an end mill through a roughing operation. In this case, the roughness profile was measured in the tool feed direction. As it is seen in the figure, irregular undulations were measured that may represent the appearance of vibrations and a more unstable machining performance. It can be concluded that the cutting performed better on the thin rigid sections (Fig. 14a) that on the overhang sections (Fig. 14b). The quantitative evaluation of the machining stability is out of the focus in this work. However, these results suggest the need for a further study and analysis of the clamping effect on the stability of AM-ed component post-processing.

Dimensional and geometrical accuracy

The dimensional and geometrical analysis in the CMM of the as-built component allowed to quantitatively assess the effect of the springback phenomenon and analyse the LPBF integrity. Critical sections were thoroughly inspected and compared with the theoretical model. As represented in Fig. 16a (by the arrows), the

Table 3
Comparison of the dimensional and geometrical deviations of the manufactured component by hybrid manufacturing.

Characteristics	Element	As-built	Post-processed
		Deviation, mm (theoretical model compares to the as-built component)	Deviation, mm (original design compares to the machined component)
Diameter	Cylinder 1	0.223 (1.3%)	0.025 (0.13%)
	Cylinder 2	0.173 (1%)	0.027 (0.13%)
	Cylinder 3	0.239 (2.5%)	0.012 (0.05%)
	Cylinder 4	0.423 (4.5%)	0.015 (0.07%)
	Cylinder 5	0.251 (2.7%)	0.012 (0.05%)
	Cylinder 6	0.154 (1.6%)	0.019 (0.09%)
Flatness	Plane 1	0.195	0.015
	Plane 2	0.175	0.018
	Plane 3	0.199	0.015
	Plane 4	0.183	0.017
	Plane 5	0.231	0.031
	Plane 6	0.211	0.035
	Plane 7	0.298	0.029
	Plane 8	0.300	0.025
Parallelism	Plane 5 (level and straight surface in XY as datum)	1.278	0.043
	Plane 6 (level and straight surface in XY as datum)	1.337	0.017
	Plane 7 (level and straight surface in XY as datum)	3.379	0.033
	Plane 8 (level and straight surface in XY as datum)	2.792	0.021
Perpendicularity	Cylinder 3 (plane 5 as datum)	0.608	0.089
	Cylinder 4 (plane 6 as datum)	0.513	0.045
	Cylinder 5 (plane 7 as datum)	0.779	0.067
	Cylinder 6 (plane 8 as datum)	0.555	0.057

distortion took place approximately in two directions by warping the four legs inwards and upwards. Since the design of the component was based on a TO, the sections are not symmetrical, so the deviation values are scattered. Fig. 16b shows the difference between the as-built diameter and thickness with the theoretical model. The location of these holes and the perpendicular surface to the built platform was beneficial in regard to the printing. Both the diameter and the thickness were slightly smaller (1.3%–1% and 0.59%–0.88%, respectively) than the theoretical model. No additional remarkable defects such as delamination or cracks were found.

Different characteristics were measured along the sections (planes and cylinder) detailed in Fig. 2. A comparative summary of the dimensional and geometrical deviations of the as-built LPBF-ed component and the machined component is shown in Table 3. Overall, in the as-built LPBF-ed component, the diameter of cylinders 1 and 2 and the flatness of planes 1, 2, 3 and 4 showed the closest agreement. These measurements belong to the rings section. The high values of the parallelism of planes 5, 6, 7 and 8 were influenced by the distortion from the thermo-mechanical phenomena during the printing process. From the comparison it can be extracted that the sections in which milling operations were carried out showed a slight deviation from the theoretical model. Although planes 5, 6, 7 and 8 were the most affected by the distortions of the legs, the flatness, and parallelism tolerance values after post-processing were still satisfactory.

Literature has reported the generation of holes in parts manufactured through LPBF process based on the orientation and dimension [47]. In most of the cases, support material is needed to build the hole properly. However, these regions are usually difficult to access; support removal will be hindered, and burrs can remain after post-processing. For instance, the four bores (named Cylinders 3, 4, 5 and 6) were the most demanding sections to inspect and machine. Therefore, it was concluded that drilling could be a good alternative to the generation of the hole in the LPBF process. The hole is constructed with solid support material that must be removed with additional cleaning operations. In addition, the perpendicularity of the bolt holes with respect to their boundary surfaces is an important feature in load-bearing structures. This tough perpendicularity requirement could not be met with AM only due to the distortions and surface defects generated. As shown in Table 3, after machining, the perpendicularity of cylinders 3, 4, 5 and 6 was greatly improved. The improvement percentage was higher than 83%, reaching values up to 97%.

Conclusions

In this work, Hybrid Additive Manufacturing was employed to manufacture a Ti6Al4V aerospace component by integrating a LPBF additive manufacturing technology and post-processing through 5-axis machining. Each of the stages in the workflow were essential to ensure good quality and accuracy. Based on the results obtained, it can be noted that the combination of both technologies enables the generation of lightweight complex geometries with good surface qualities and dimensional and geometrical accuracy in critical sections. The following conclusions were drawn from this study:

- When working with this hybrid approach, both the requirements for additive and subtractive processes must be considered from the initial design stage. In this work, the topologically optimised model of the component was adapted to the hybrid approach by adding an allowance in the critical sections that were later to be machined. This helped in alleviating the superficial and geometrical defects. Additionally, considering the need for clamping during the machining stage, a section was added to the optimised design, making it possible to complete all the needed milling operations in a single setup. Those features represent a slight material increase that can be neglected when compared to the overall weight reduction obtained.
- The generation of residual stresses, which in turn, induce distortion on the component, was inherent to additive processes since thermal cycles occurred during the deposition of successive layers. The manufacturing of an end-use component with good surface quality and dimensional accuracy by AM only is still far off.
- The FEM simulation conducted provided a better understanding of the residual stress behaviour and its influence on the distortions generated in LPBF-ed components. It was validated that the highest distortions occurred in the stress relaxation stage once the as-built part was separated from the substrate. A heat treatment applied before the separation of the sample from the substrate can help to mitigate the residual stresses and, in turn, the distortions.
- From the FEM simulation it was noted that the support structures play an important role in the LPBF process, as they help to mitigate the heat generated and reduce distortion. However from the analysis of the as-built part, it was found that they also increase the surface roughness once they are removed from the component. This conclusion highlights the need for future research on the influence of the amount, location and geometry of support structures on residual stress distributions, part distortion and surface quality.
- Regarding the surface quality of the as-built part, it was observed that orientation during deposition has a great effect on the results. In comparing upward- and downward-facing surfaces, the latter are more prone to result in a rougher surface. Previous works suggest specific values of built angles to control this effect. However, a strategy based on built orientation is not feasible in the manufacturing of a component such as the one studied in this work.
- Despite the low machinability of Ti6Al4V alloy, the adopted machining strategy was effective. After post-processing the as-built component through 5-axis milling the surface quality was greatly improved, as so were the geometrical and dimensional accuracy. Machining instability was mainly present on the overhang sections. This conclusion remarks the need to further analyze the effect of clamping and component rigidity on machining performance in order to optimise the post-processing stage and the overall results.
- The low quality and dimensional distortion of the as-built small inner channels or holes suggests that a drilling operation should have been performed instead of printing. The support structured needed for the generation of this small holes during the additive process deteriorated the hole surface quality and dimensional accuracy.

Declaration of Competing Interest

The authors declare that they have no known competing financial interests or personal relationships that could have appeared to influence the work reported in this paper.

Acknowledgements

We gratefully acknowledge the support for this study by the Regional Council of Gipuzkoa.

References

[1] Huang, R., Riddle, M., Graziano, D., Warren, J., Das, S., Nimbalkar, S., et al., 2016, Energy and Emissions Saving Potential of Additive Manufacturing: the Case of Lightweight Aircraft Components. The Journal of Cleaner Production, 135:1559–1570. https://doi.org/10.1016/j.jclepro.2015.04.109.

[2] Allen, J., 2006. An Investigation Into the Comparative Costs of Additive Manufacture Vs. Machine from Solid for Aero Engine Parts, in: Cost Effective Manufacture via Net-Shape Processing, Meeting Procedings RTO-MP-AVT-139, 17-1 - 17-10.

[3] Stavropoulos, P., Bikas, H., Avram, O., Valente, A., Chryssolouris, G., 2020, Hybrid Subtractive–additive Manufacturing Processes for High Value-added Metal Components. International Journal of Advanced Manufacturing Technology, 111:645–655. https://doi.org/10.1007/s00170-020-06099-8.

[4] Leary, M., 2017, Surface Roughness Optimisation for Selective Laser Melting (SLM). Laser Additive Manufacturing. Elsevier: 99–118. https://doi.org/10.1016/B978-0-08-100433-3.00004-X.

[5] Ni, C., Zhu, L., Zheng, Z., Zhang, J., Yang, Y., Hong, R., et al., 2020, Effects of Machining Surface and Laser Beam Scanning Strategy on Machinability of Selective Laser Melted Ti6Al4V Alloy in Milling. Materials and Design, 194:108880https://doi.org/10.1016/j.matdes.2020.108880.

[6] Ni, C., Zhu, L., Zheng, Z., Zhang, J., Yang, Y., Yang, J., et al., 2020, Effect of Material Anisotropy on Ultra-precision Machining of Ti-6Al-4V Alloy Fabricated by Selective Laser Melting. The Journal of Alloys and Compounds, 848:156457https://doi.org/10.1016/j.jallcom.2020.156457.

[7] Jiménez, A., Bidare, P., Hassanin, H., Tarlochan, F., Dimov, S., Essa, K., 2021, Powder-based Laser Hybrid Additive Manufacturing of Metals: A Review. International Journal of Advanced Manufacturing Technology, 114:63–96. https://doi.org/10.1007/s00170-021-06855-4.

[8] Gokuldoss, P.K., Kolla, S., Eckert, J., 2017, Additive Manufacturing Processes: Selective Laser Melting, Electron Beam Melting and Binder Jetting-selection Guidelines. Materials, 10. https://doi.org/10.3390/ma10060672.

[9] Liu, S., Shin, Y.C., 2019, Additive Manufacturing of Ti6Al4V Alloy: A Review. Materials and Design, 164:107552https://doi.org/10.1016/j.matdes.2018.107552.

[10] Xiao, Z., Chen, C., Zhu, H., Hu, Z., Nagarajan, B., Guo, L., et al., 2020, Study of Residual Stress in Selective Laser Melting of Ti6Al4V. Materials and Design, 193:108846https://doi.org/10.1016/j.matdes.2020.108846.

[11] Keller, N., Ploshikhin, V., 2014. New Method for Fast Predictions of Residual Stress and Distortion of AM Parts. In: Proceedings of the 25th Annual International Solid Freeform Fabrication Symposium: An Additive Manufacturing Conference, SFF 2014, pp. 1229–1237.

[12] Mercelis, P., Kruth, J.P., 2006, Residual Stresses in Selective Laser Sintering and Selective Laser Melting. Rapid Prototyping Journal, 12:254–265. https://doi.org/10.1108/13552540610707013.

[13] Bartlett, J.L., Li, X., 2019, An Overview of Residual Stresses in Metal Powder Bed Fusion. Additive Manufacturing, 27:131–149. https://doi.org/10.1016/j.addma.2019.02.020.

[14] Carpenter, K., Tabei, A., 2020, On Residual Stress Development, Prevention, and Compensation in Metal Additive Manufacturing. Materials, 13. https://doi.org/10.3390/ma13020255.

[15] Yılmaz, N., Kayacan, M.Y., 2021, Effect of Single and Multiple Parts Manufacturing on Temperature-induced Residual Stress Problems in SLM. International Journal of Material Forming, 14:407–419. https://doi.org/10.1007/s12289-020-01560-1.

[16] Denlinger, E.R., Michaleris, P., 2016, Effect of Stress Relaxation on Distortion in Additive Manufacturing Process Modeling. Additive Manufacturing, 12:51–59. https://doi.org/10.1016/j.addma.2016.06.011.

[17] Shipley, H., McDonnell, D., Culleton, M., Coull, R., Lupoi, R., O'Donnell, G., et al., 2018, Optimisation of Process Parameters to Address Fundamental Challenges during Selective Laser Melting of Ti-6Al-4V: A Review. The International Journal of Machine Tools and Manufacture, 128:1–20. https://doi.org/10.1016/j.ijmachtools.2018.01.003.

[18] Leary, M., 2018, Design of Titanium Implants for Additive Manufacturing. Titanium in Medical and Dental Applications. Elsevier: 203–224. https://doi.org/10.1016/B978-0-12-812456-7.00009-3.

[19] Gupta, R.K., Kumar, V.A., Mathew, C., Rao, G.S., 2016, Strain Hardening of Titanium Alloy Ti6Al4V Sheets with Prior Heat Treatment and Cold Working. Materials Science and Engineering: A, 662:537–550. https://doi.org/10.1016/j.msea.2016.03.094.

[20] Prasad AVSR, Ramji Koona, Datta, G.L., 2014, An Experimental Study of Wire EDM on Ti-6Al-4V Alloy. Procedia Materials Science, 5:2567–2576. https://doi.org/10.1016/j.mspro.2014.07.517.

[21] Ghiotti, A., Bertolini, R., Sorgato, M., Campagnolo, A., Savio, E., Bruschi, S., 2022, Ti6Al4V Titanium Alloy Fatigue Strength after AM- and Machining-based Process Chains. CIRP Annals, 71:461–464. https://doi.org/10.1016/j.cirp.2022.04.021.

[22] Dutta, B., Froes, F.H., 2017, Chapter 1—The Additive Manufacturing of Titanium Alloys. Dutta B, Froes FH, (Eds.) Additive Manufacturing of Titanium Alloys. Elsevier, Amsterdam, The Netherlands.

[23] Yang, J., Yu, H., Yin, J., Gao, M., Wang, Z., Zeng, X., 2016, Formation and Control of Martensite in Ti-6Al-4V Alloy Produced by Selective Laser Melting. Materials and Design, 108:308–318. https://doi.org/10.1016/j.matdes.2016.06.117.

[24] Liu, S., Shin, Y.C., 2019, Additive Manufacturing of Ti6Al4V Alloy: A Review. Materials and Design, 164:107552https://doi.org/10.1016/j.matdes.2018.107552.

[25] Veiga, C., Davim, J.P., Loureiro, A.J.R., 2012, Properties and Applications of Titanium Alloys: A Brief Review. Reviews on Advanced Materials Science, 32:133–148.

[26] Liu, S., Shin, Y.C., 2019, Additive Manufacturing of Ti6Al4V Alloy: A Review. Materials and Design, 164:107552https://doi.org/10.1016/j.matdes.2018.107552.

[27] Veiga, C., Davim, J.P., Loureiro, A.J.R., 2013, Review on Machinability of Titanium Alloys: the Process Perspective. Reviews on Advanced Materials Science, 34:148–164.

[28] Ribeiro, M.V., Moreira, M.R.V., Ferreira, J.R., 2003, Optimization of Titanium Alloy (6Al–4V) Machining. Journal of Materials Processing Technology, 143–144:458–463. https://doi.org/10.1016/S0924-0136(03)00457-6.

[29] Campbell Jr., F.C., 2006, Manufacturing Technology for Aerospace Structural Materials. Elsevier. https://doi.org/10.1016/B978-1-85617-495-4.X5000-8.

[30] Maleki, E., Bagherifard, S., Bandini, M., Guagliano, M., 2021, Surface Post-treatments for Metal Additive Manufacturing: Progress, Challenges, and Opportunities. Additive Manufacturing, 37:101619https://doi.org/10.1016/j.addma.2020.101619.

[31] Pakkanen, J., Calignano, F., Trevisan, F., Lorusso, M., Ambrosio, E.P., Manfredi, D., et al., 2016, Study of Internal Channel Surface Roughnesses Manufactured by Selective Laser Melting in Aluminum and Titanium Alloys. Metallurgical and Materials Transactions A: Physical Metallurgy and Materials Science, 47:3837–3844. https://doi.org/10.1007/s11661-016-3478-7.

[32] Zhang, B., Yuan, J., Wang, Z., Li, X., 2022, Precise Machining Based on Ritz Non-uniform Allowances for Titanium Blade Fabricated by Selective Laser Melting. The International Journal of Advanced Manufacturing Technology, 119:6029–6044. https://doi.org/10.1007/s00170-022-08701-7.

[33] Yaghi, A., Ayvar-Soberanis, S., Moturu, S., Bilkhu, R., Afazov, S., 2019, Design Against Distortion for Additive Manufacturing. Additive Manufacturing, 27:224–235. https://doi.org/10.1016/j.addma.2019.03.010.

[34] GE Jet Engine Bracket Challenge, n.d. ⟨https://grabcad.com/challenges/ge-jet-engine-bracket-challenge⟩. (Accessed 24 January 2022).

[35] Kranz, J., Herzog, D., Emmelmann, C., 2015, Design Guidelines for Laser Additive Manufacturing of Lightweight Structures in TiAl6V4. The Journal of Laser Applications, 27:S14001https://doi.org/10.2351/1.4885235.

[36] An, N., Yang, G., Yang, K., Wang, J., Li, M., Zhou, J., 2021, Implementation of Abaqus User Subroutines and Plugin for Thermal Analysis of Powder-bed Electron-beam-melting Additive Manufacturing Process. Materials Today Communications, 27:102307https://doi.org/10.1016/j.mtcomm.2021.102307.

[37] Liu, M., Chiu, L.N.S., Vundru, C., Liu, Y., Huang, A., Davies, C., et al., 2021, A Characteristic Time-based Heat Input Model for Simulating Selective Laser Melting. Additive Manufacturing, 44:102026https://doi.org/10.1016/j.addma.2021.102026.

[38] Yan, X., Yin, S., Chen, C., Huang, C., Bolot, R., Lupoi, R., et al., 2018, Effect of Heat Treatment on the Phase Transformation and Mechanical Properties of Ti6Al4V Fabricated by Selective Laser Melting. The Journal of Alloys and Compounds, 764:1056–1071. https://doi.org/10.1016/j.jallcom.2018.06.076.

[39] Stavropoulos, P., Souflas, T., Porevopoulos, N., Bikas, H., 2021, Application of Virtual Engineering Tools to Support Design Optimization: A Case Study on A Cryogenic Machining System. Procedia CIRP, 100:181–186. https://doi.org/10.1016/j.procir.2021.05.052.

[40] Hussein, A., Hao, L., Yan, C., Everson, R., 2013, Finite Element Simulation of the Temperature and Stress Fields in Single Layers Built Without-support in Selective Laser Melting. Materials and Design, 52:638–647. https://doi.org/10.1016/j.matdes.2013.05.070.

[41] Yadroitsev, I., Yadroitsava, I., 2015, Evaluation of Residual Stress in Stainless Steel 316L and Ti6Al4V Samples Produced by Selective Laser Melting. Virtual and Physical Prototyping, 10:67–76. https://doi.org/10.1080/17452759.2015.1026045.

[42] Gan, M.X., Wong, C.H., 2016, Practical Support Structures for Selective Laser Melting. Journal of Materials Processing Technology, 238:474–484. https://doi.org/10.1016/j.jmatprotec.2016.08.006.

[43] Yasa, E., Poyraz, O., Solakoglu, E.U., Akbulut, G., Oren, S., 2016, A Study on the Stair Stepping Effect in Direct Metal Laser Sintering of a Nickel-based Superalloy. Procedia CIRP, 45:175–178. https://doi.org/10.1016/j.procir.2016.02.068.

[44] Chen, Z., Wu, X., Tomus, D., Davies, C.H.J., 2018, Surface Roughness of Selective Laser Melted Ti-6Al-4V Alloy Components. Additive Manufacturing, 21:91–103. https://doi.org/10.1016/j.addma.2018.02.009.

[45] Yang, T., Liu, T., Liao, W., Wei, H., Zhang, C., Chen, X., et al., 2021, Effect of Processing Parameters on Overhanging Surface Roughness during Laser Powder Bed Fusion of AlSi10Mg. Journal of Manufacturing Processes, 61:440–453. https://doi.org/10.1016/j.jmapro.2020.11.030.

[46] Bagehorn, S., Wehr, J., Maier, H.J., 2017, Application of Mechanical Surface Finishing Processes for Roughness Reduction and Fatigue Improvement of Additively Manufactured Ti-6Al-4V Parts. The International Journal of Fatigue, 102:135–142. https://doi.org/10.1016/j.ijfatigue.2017.05.008.

[47] Ming, W., Dang, J., An, Q., Chen, M., 2020, Chip Formation and Hole Quality in Dry Drilling Additive Manufactured Ti6Al4V. Materials and Manufacturing Processes, 35:43–51. https://doi.org/10.1080/10426914.2019.1692353.